Environ. Sci. Technol. **2000**, *34,* 950−958

Quantitative Speciation of Mn-Bearing Particulates Emitted from Autos Burning (Methylcyclopentadienyl)manganese Tricarbonyl-Added Gasolines Using XANES Spectroscopy

THORSTEN RESSLER,[†,‡] JOE WONG,[*,†] JOSEPH ROOS,[§] AND ISSAC L. SMITH[§]

Lawrence Livermore National Laboratory, University of California, P.O. Box 808, Livermore, California 94551, Department of Inorganic Chemistry, Fritz-Haber-Institute of the Max-Planck-Society, Faradayweg 4-6, D-14195 Berlin, Germany, and R&D Center, Ethyl Corporation, P.O. Box 2189, Richmond, Virginia 23217

The chemical nature of Mn-containing particulates emitted from (methylcyclopentadienyl)manganese tricarbonyl-added gasoline engines has been elucidated using Mn K-edge X-ray absorption fine structure (XAFS) spectroscopy. Edge shift data from the X-ray absorption near-edge structure (XANES) spectra showed that the average Mn valence in these particulates is ∼2.2. Using a principal component analysis (PCA) algorithm, the number and type of probable species contained in these particulates were determined to be three, consisting of Mn_3O_4, $MnSO_4 \cdot H_2O$, and a divalent manganese phosphate, $Mn_5(PO_4)[PO_3(OH)]_2 \cdot 4H_2O$. The proportions of these Mn phases in each particulate sample were evaluated quantitatively using least-squares fitting (LSF) of the experimental XANES spectra with linear combinations of these principal component (model compound) spectra. Two groups of Mn-bearing particulates may be distinguished: group I having 4−9 wt % of Mn_3O_4 and exhibiting a single intense first major absorption maximum at the Mn K-edge and group II containing 15−22 wt % of Mn_3O_4 and exhibiting a doublet absorption maximum at lower intensity. Fourier transforms of the EXAFS signals were found to corroborate the XANES results. This study clearly establishes XANES spectroscopy, in combination with PCA and LSF, as a quantitative analytical tool for speciation of dilute and/or amorphous multicomponent environmental materials not easily attainable with conventional methods.

Introduction

The potential health effects of airborne particulate matter (PM) have recently prompted considerable debate. This debate centers upon the efficacy of new PM standards proposed by the U.S. Environmental Protection Agency (EPA) given the high cost estimated to achieve the new PM standard (*1*). To date, there is little information about the chemical nature of PM or the health effects associated with PM in outdoor or indoor air. Upon recommendation of the National Academy of Sciences and congressional mandate, the EPA has expanded its efforts to obtain detailed knowledge about particulate matter with the goal of implementing control measures for PM on a more solid and sound scientific basis.

One important research topic concerns the identification of chemical species in PM and the methods used to evaluate particulate chemical composition. This information could prove very important when addressing source apportionment issues and evaluating the effect of PM on air quality. The present work was undertaken to develop a spectroscopic tool to speciate compounds that exist in dilute and/or amorphous phases within airborne particulates. The subject of the work is Mn-bearing materials emitted from vehicles operating on fuels containing a manganese-based fuel additive.

(Methylcyclopentadienyl)manganese tricarbonyl (MMT) is a fuel additive for enhancing fuel efficiency and decreasing emission in automobiles. Environmental concerns about airborne Mn-bearing particulates and their potential health effects require intensive studies regarding the form and distribution of manganese emitted from the automotive engine (*2*). The effect of using MMT-containing gasoline on vehicle emissions along roadways (*3*) and ambient manganese levels (*4*) have been the subject of extensive study. In the period 1990−1994, a series of assessments of the potential health risks associated with the use of an MMT additive in unleaded gasoline was performed by the EPA (*5, 6*). These led to the identification of a key health issue associated with inhalation exposure to Mn-bearing particulates resulting from the combustion of MMT in gasoline. A number of research areas have also been proposed to address potential manganese exposures associated with use of MMT, toxicological end points, as well as certain pharmacokinetic and emission characterization issues (*7*). Moreover, it is well-known that certain species of manganese are highly soluble and other species are not. Thus, depending on the species of manganese inhaled, more or less manganese may be absorbed into the blood. In addition, it has been suggested that differences in the valence state of inhaled manganese may result in differences in distribution or toxicity (*6*). It is important, therefore, to determine the composition of actual Mn-bearing particulates emitted by vehicles burning fuels containing MMT. The chemical knowledge is a prerequisite to pharmacokinetic studies for appropriate choice of atmosphere and other issues pertaining to the design of animal testing, such as proper dosage to provide insight into which species of manganese are most problematic in terms of delivery to the brain.

X-ray diffraction measurements (*8*) yielded little or no information due to a combination of insufficient sample mass, amorphous nature of the particulate matter, and/or small particle size. Studies of four relatively heavily loaded samples (292−4244 μg) showed only background from the filter substrate material. ESCA measurements identified O, P, and S as major elements likely to be associated with the Mn-bearing exhaust particulates. Mn, P, and S 2p and O 1s core-level spectroscopy indicated that the vehicle exhaust may contain manganese primarily in the form of a manganese phosphate and/or sulfate (*8*). Thus, the physiochemical nature of these Mn-bearing exhaust particulates is largely unknown and not well-characterized.

XAFS (X-ray absorption fine structure) spectroscopy (*9*) using intense synchrotron radiation appears to be the method

* Corresponding author phone: (925)423-6385; fax: (925)424-4737; e-mail: Wong10@LLNL.gov.
† University of California.
‡ Fritz-Haber-Institute of the Max-Planck-Society.
§ Ethyl Corporation.

10.1021/es990787x CCC: $19.00 © 2000 American Chemical Society
Published on Web 02/08/2000

TABLE 1. History of Mn-Bearing Particulates: Vehicle, Mileage Accumulation, and Test Cycle Used

no.	vehicle	mileage	test cycle	edge jump (μx)	E_0 position[b] (eV)	valence	1st absorption[c] max (μx)	group
1	A	4 000	FTP extended	0.045	7.68	2.12	1.64	I
2	A	4 000	UDC	0.075	7.57	2.08	1.57	I
3	A	40 000	FTP extended	0.040	7.65	2.11	1.58	I
4	A	40 000	UDC	0.140	7.78	2.14	1.55	I
5	B	4 000	FTP	0.090	7.83	2.16	1.48	I
6	B	4 000	FTP inactive catalyst	0.030	7.86	2.17	1.61	I
7	B	4 000	FTP extended	0.340	7.93	2.19	1.39	II
8	B	4 000	UDC	0.500	7.80	2.15	1.42	II
9	B	40 000	FTP	0.150	7.84	2.16	1.28	II
10	B	40 000	FTP inactive catalyst	0.050	7.89	2.18	1.48	I
11	B	40 000	FTP extended	0.050	7.77	2.14	1.56	I
12	B	40 000	UDC	0.900	7.83	2.16	1.33	II

[a] The observed XANES spectral features tabulated here are discussed in the text. [b] E_0 is measured with respect to the Mn metal K-edge at 6539 eV. [c] From normalized XANES spectra.

of choice for chemical speciation of PM and other environmental materials that are generally low in concentration and/or small total sample size. This technique is atomic specific and sensitive to low concentration (10 ppm or lower) as well as low sample mass ($\sim\mu$g with third generation synchrotron sources). Sample crystallinity is not required since XAFS is a structural probe sensitive to short-range order. Chemical information such as valence, coordination geometry, bond distance, and ligand coordination number can be obtained with high accuracy in combination with use of appropriate model compounds and theoretical FEFF simulations (*10*, *11*). Furthermore, this tool can now be rendered quantitative in multicomponent systems of environmental concern (*12*−*16*) and with uniqueness as is demonstrated in this work.

We have, therefore, applied Mn K-edge XAFS spectroscopy to characterize exhaust particulates sampled in a controlled manner from a pair of sister vehicles running MMT-containing gasoline and various EPA standardized test cycles. Using a set of preselected manganese model compounds, the Mn-bearing components in the exhaust particulates were speciated by first utilizing a PCA algorithm to determine the minimum number and type of probable components and then quantified from the experimental XANES spectra using a least-squares fitting (LSF) procedure. Analysis of the EXAFS spectra at higher energies using the standard Fourier transform procedure has been used to substantiate findings from the XANES data.

Experimental Section

Particulate Samples. The Mn-bearing particulate samples were collected at Southwest Research Institute in San Antonio, TX. Teflon-coated fiber glass filters 47 mm in diameter were used. Two identical 1997 Ford Taurus vehicles (3.0-L V6), denoted as vehicles A and B, were employed to generate the particulates under four test cycles. Samples were collected after 4000 and 40 000 mi of operation on gasoline containing MMT at 0.03125 g of Mn/gal. The 12 particulate samples collected from these two vehicles using the various driving cycles and at the different mileage points are listed in Table 1.

Samples were collected during the FTP (federal test procedure) test cycle. This cycle is comprised of a cold start, a 505-s transient phase, a 867-s stabilized phase, and a 600-s engine-off soak. After the soak, the vehicle was started with a hot engine and repeated the transient and stabilized phase of operation. This period was equivalent to a 15-m travel for the vehicle. This cycle was repeated on three consecutive days. Each day, testing began with the cold start. Sample collection was also performed during extended operation of the FTP (FTP extended). During this operation, the FTP was run as described above. After the completion of the second stabilized phase, the vehicle was subjected to a 600-s engine-off soak. After the soak, the transient and stabilized cycle was repeated 13 additional times. Each repeat was separated by the 600-s engine-off soak. The total run time for each FTP test was 343 min or 5 h and 43 min. A more severe California Unified Driving Cycle (UDC) as recommended by the EPA was also used. This driving cycle contains higher speeds and accelerations than found in the FTP cycles. After a cold start, bags 1 and 2 of the UDC were repeated 14 times. Each repetition was separated by a 600-s soak followed by a hot starts. Over the UDC cycle, the vehicle operated an equivalent of 137-mi travel. The FTP inactive catalyst test cycle was similar to the normal FTP except that the inactive catalyst was placed on the vehicle.

Model Compounds. These include a series of manganese oxides and oxyhydroxides: MnO, Mn_2O_3, Mn_3O_4, β-MnO_2, and α-MnO(OH); selected divalent salts: MnS, $MnSO_4{\cdot}H_2O$, $Mn_2P_2O_7$, and $Mn_5(PO_4)[PO_3(OH)]_2{\cdot}4H_2O$ (hureaulite, abbreviation MnPhos used in this paper); and trivalent $MnPO_4$. The choice of these model compounds was guided by ESCA identification (*8*) of O, P, and S associated with the exhaust particulates as well as thermodynamic considerations at the fuel combustion conditions (*17*). The oxides, sulfate, MnPhos, and $MnPO_4$ were procured from Alfa Aesar; MnS was from Aldrich; and manganese metal powder was from Cerac. $Mn_2P_2O_7$ was synthesized by heating $MnPO_4$ at 700 °C for 19 h. The phase purity of these model compounds was examined using in-house X-ray powder diffractometry, which showed no detectable impurity Bragg lines in each material used.

XAFS Measurements. XAFS measurements were performed on beamline 10-2 (*18*) at Stanford Synchrotron Radiation Laboratory (SSRL) with SPEAR (Stanford Positron Electron Accumulation Ring) operating at an electron energy of 3.0 GeV and injection current at ~100 mA. The synchrotron beam from the wiggler was apertured with a 0.5-mm vertical entrance slit and monochromatized using a Si(220) double crystal, which was 50% detuned to minimize higher harmonics. For bulk model compounds, a conventional transmission mode was used to collect the absorption spectra. For the particulate specimens with low Mn concentration, a fluorescence detection mode utilizing a Lytle detector was used (*19*). The monochromatic beam incident on the sample at 45° had a footprint 2 mm high × 28 mm wide for maximum sample coverage. All spectra were collected in the QEXAFS mode (*20*). Multiple scans varying from 4 sweeps for XANES and 8 sweeps for EXAFS were performed to ~1000 eV (~16 $Å^{-1}$) above the Mn K-edge to yield optimal S/N ratios. An equivalent step size of 0.25 eV/point was used for XANES scans, and one of 1.0 eV/point was used for EXAFS scans. A

manganese metal standard foil located in front of a reference ion chamber was measured simultaneously with each spectral sample for in-situ energy calibration.

Data Analysis

Energy Calibration and Normalization. Data reduction of experimental XAFS spectra was carried out using the software WinXAS97 v1.2 (*21*). The energy threshold $E_{0,\mathrm{ref}}$ of the reference metal foil was determined from the first inflection point in the spectrum (*22*), and raw data were linearly calibrated against the difference between the obtained $E_{0,\mathrm{ref}}$ and the tabulated absorption edge energy for Mn K edge at 6.539 keV (*23*). Pre-edge background subtraction and XANES normalization were carried out by fitting a linear polynomial to the pre-edge region and a cubic polynomial to the postedge region of the absorption spectrum. A smooth atomic background, $\mu_0(k)$, was obtained using cubic splines. The radial distribution function FT[$(\chi(k)$] was obtained by Fourier transforming the k^3-weighted experimental $\chi(k)$ function multiplied by a Bessel window into the *R* space.

The normalized XANES spectra of the Mn speculate samples were analyzed with a two-step procedure, each utilizing a different mathematical algorithm: (i) determination of the number of constituent species in the unknown samples and identification of suitable species from the chosen model compounds using principal component analysis (PCA) and (ii) quantification of the identified species in each unknown particulate sample with nonlinear least-squares refinements.

PCA. In the analysis of a set of XANES spectra arising from mixtures (superimpositions) of spectra from two or more different reference compounds, PCA can be employed to determine the number of reference model spectra needed to simulate the experimental data. In addition, given a set of spectra of suitable reference model compounds, PCA in combination with target transformation (discussed later) can be utilized to identify those model compounds that constitute probable components in the original set of unknown XANES spectra. It must be noted that the number of compounds present in the measured XANES spectra of unknowns has to be equal or smaller than the number of spectra.

The PCA procedure employed in this work to determine the minimum number and type of Mn species contained in an unknown Mn-bearing particulate sample from a suitable preselected set of reference compounds has been applied to XAFS analysis by Fay et al. (*24*) and reiterated in detail more recently by Wasserman (*25*). This procedure is based on the singular value decomposition (SVD) algorithm (*26*, *27*) in linear algebra, which is briefly described as follows.

The SVD method is based on the theorem that any $m \times n$ matrix **A**, whose number of rows *m* is greater than or equal to its number of columns *n*, can be written as the product of an $m \times n$ column-orthogonal matrix **E**, an $n \times n$ diagonal matrix **V** with positive or zero elements, and the transpose of an $n \times n$ orthogonal matrix **w** (*28*, *29*). The columns of the **E** matrix are the eigenvectors, and the diagonal elements of the **V** matrix are the corresponding eigenvalues.

$$\begin{bmatrix} x_{11} & x_{12} & \cdots & x_{1n} \\ a_{21} & a_{22} & \cdots & a_{2n} \\ n_{31} & n_{32} & \cdots & n_{3n} \\ e_{41} & e_{42} & \cdots & e_{4n} \\ \cdot & \cdot & \cdots & \cdot \\ \cdot & \cdot & \cdots & \cdot \\ \cdot & \cdot & \cdots & \cdot \\ s_{m1} & s_{m2} & \cdots & s_{mn} \end{bmatrix} = \begin{bmatrix} E_{11} & E_{12} & \cdots & E_{1n} \\ i_{21} & i_{22} & \cdots & i_{2n} \\ g_{31} & g_{32} & \cdots & g_{3n} \\ e_{41} & e_{42} & \cdots & e_{4n} \\ \cdot & \cdot & \cdots & \cdot \\ \cdot & \cdot & \cdots & \cdot \\ \cdot & \cdot & \cdots & \cdot \\ n_{m1} & n_{m2} & \cdots & n_{mn} \end{bmatrix} \bullet \begin{bmatrix} v_{11} & 0 & \cdots & 0 \\ 0 & v_{22} & \cdots & 0 \\ \cdot & \cdot & v_{ii} & \cdot \\ 0 & 0 & \cdots & v_{nn} \end{bmatrix} \bullet \begin{bmatrix} w_{11} & w_{12} & \cdots & w_{1n} \\ w_{21} & w_{22} & \cdots & w_{2n} \\ \cdot & \cdot & \cdots & \cdot \\ w_{n1} & w_{n2} & \cdots & w_{nn} \end{bmatrix}$$

$$[A] = [E] \bullet [V] \bullet [w]^t \qquad (1)$$

Thus, SVD constructs an orthonormal basis set given as column vectors of the **E** matrix in eq 1 from the vector subspace spanned by the input column vectors of the **A** matrix. In practice, therefore, column vector (x_{1j}, a_{2j}, n_{3j}, e_{4j}, ..., s_{mj}) in matrix **A** represents an experimental XANES spectrum of the *j*th unknown mixture, and there are *n* such unknown spectra in the data set to be analyzed, each with *m* data points. The output matrix **E** has, therefore, a dimension *n*, which is the number of columns in the input matrix **A**. Oftentimes, however, eigenvalues v_{ii} equal to zero indicate that the subspace spanned by the input vectors was not, in fact, *n*-dimensional. The columns of **E** that correspond to zero, v_{ii}, should then be discarded from the orthonormal basis set.

To use the above-described SVD algorithm, a column matrix **A** has to be constructed containing the experimental XANES spectra interpolated onto the same energy grid. From the eigenvalues in the SVD output matrix **V**, it can be determined how many eigenvectors are sufficient to reproduce the experimental XANES spectra; hence, the number of principal components present in the experimental data set. In eq 2, for instance, if two out of the *n* eigenvectors in

$$\begin{bmatrix} E_{11} & E_{12} & \cdots & E_{1n} \\ i_{21} & i_{22} & \cdots & i_{2n} \\ g_{31} & g_{32} & \cdots & g_{3n} \\ e_{41} & e_{42} & \cdots & e_{4n} \\ \cdot & \cdot & \cdots & \cdot \\ \cdot & \cdot & \cdots & \cdot \\ \cdot & \cdot & \cdots & \cdot \\ n_{m1} & n_{m2} & \cdots & n_{mn} \end{bmatrix} \bullet \begin{bmatrix} v_{11} & 0 & 0_{ii} & 0_{1n} \\ 0 & v_{22} & 0_{ii} & 0_{1n} \\ 0 & 0 & 0_{ii} & 0 \\ 0 & 0 & 0_{ni} & 0_{nn} \end{bmatrix} \bullet \begin{bmatrix} w_{11} & w_{12} & \cdots & w_{1n} \\ w_{21} & w_{22} & \cdots & w_{2n} \\ \cdot & \cdot & \cdots & \cdot \\ w_{n1} & w_{n2} & \cdots & w_{nn} \end{bmatrix} = \begin{bmatrix} x_{11}^* & x_{12}^* & \cdots & x_{1n}^* \\ a_{21}^* & a_{22}^* & \cdots & a_{2n}^* \\ n_{31}^* & n_{32}^* & \cdots & n_{3n}^* \\ e_{41}^* & e_{42}^* & \cdots & e_{4n}^* \\ \cdot & \cdot & \cdots & \cdot \\ \cdot & \cdot & \cdots & \cdot \\ \cdot & \cdot & \cdots & \cdot \\ s_{m1}^* & s_{m2}^* & \cdots & s_{mn}^* \end{bmatrix}$$

$$[E]^{PCA} \bullet [V]^{PCA} \bullet [w]^t = [A^*]^{PCA} \qquad (2)$$

eq 1 are needed to generate a column matrix **A*** containing the *n* PCA-calculated XANES spectra and if the columns in **A*** and **A** are identical within experimental errors, then the experimental XANES spectra in matrix **A** indeed consist of only two principal components.

The output of SVD can now be utilized to determine whether a particular vector *T* lies within the vector subspace spanned by the orthonormal basis vectors, i.e., the eigenvectors or principal components. This procedure is known as target tranformation. With respect to the case discussed in the preceding paragraph and provided the vector *T* has been interpolated onto the same grid as the number of rows *m* of the *A* matrix, a target transformation consists of a multiplication of a column matrix **E** containing the eigenvectors, the transpose of this matrix, and the vector *T* as shown in eq 3. If *T** and *T* are identical within experimental

$$\begin{pmatrix} T_1^* \\ e_2^* \\ s_3^* \\ t_4^* \\ \cdot \\ \cdot \\ \cdot \\ v_m^* \end{pmatrix} = \begin{bmatrix} E_{11} & E_{12} \\ i_{21} & i_{22} \\ g_{31} & g_{32} \\ e_{41} & e_{42} \\ \cdot & \cdot \\ \cdot & \cdot \\ \cdot & \cdot \\ n_{m1} & n_{m2} \end{bmatrix} \bullet \begin{bmatrix} E_{11} & i_{21} & g_{31} & e_{41} & \cdots & n_{m1} \\ E_{12} & i_{22} & g_{32} & e_{42} & \cdots & n_{m2} \end{bmatrix} \bullet \begin{pmatrix} T_1 \\ e_2 \\ s_3 \\ t_4 \\ \cdot \\ \cdot \\ \cdot \\ v_m \end{pmatrix}$$

$$(T^*) = [E] \bullet [E]^t \bullet (T) \qquad (3)$$

errors, the vector *T* is indeed included in the vector subspace and is a principal component of the input vector set given in the column vectors of matrix **A**.

Finally, to utilize target transformation, an XANES spectrum of a pure reference compounds after interpolation onto the same energy grid as the unknown spectra may be multiplied with the eigenvector column matrix according to eq 3. A good agreement (direct superimposition, with a residual <1.0%, for example) of the reference spectrum (*T* in eq 3) and the resulting vector (*T** in eq 3) indicates that this particular reference compound is a probable species in the unknown mixture. To assess the attainable accuracy of the PCA method, SVD and target transformation have been carried out for four XANES spectra of synthetic mechanical mixtures with varying amounts of MnO and Mn_3O_4. The target

transformation result for MnO in this ideal case is indeed indistinguishable from the experimental spectrum as expected.

LSF of XANES Spectra. On the basis of the obtained PCA results in terms of number and probable type of constituent (reference) species in the exhaust particulates, a LSF procedure was then applied to determine the amount of each reference in the particulate sample. Therefore, a sum of the reference spectra was refined to each particulate XANES spectra. The employed nonlinear LSF procedure is based on the Levenberg−Marquardt algorithm (*27*) to minimize the difference between the experimental and the simulated XANES spectrum. A fit residual R is calculated from

$$R = \frac{\sum_{i=1}^{m} |\mu_{i,\mathrm{Exp}}(E) - \mu_{i,\mathrm{Sim}}(E)|}{\sum_{i=1}^{m} |\mu_{i,\mathrm{Exp}}(E)|} \times 100 \qquad (4)$$

with $\mu_{i,\mathrm{Exp}}(E)$ as the normalized absorption of the unknown sample and $\mu_{i,\mathrm{Sim}}(E)$ as the simulated absorption based on varying amounts of normalized reference XANES spectra.

Two free running parameters were refined for each reference spectra in the least-squares XANES fits, i.e., the partial concentration and an edge-energy correction term. The latter was included to account for minor errors in energy calibration of both the unknown spectrum and the references. A conservative estimate for errors in energy calibration is the experimental step size of the XANES spectrum. Thus, edge-energy correction terms for individual references should not be much larger than this step size. In addition, this edge-energy correction term may be used to recognize references that mathematically improve the refinement but that are not present in the unknown spectrum. In the case where the edge-energy shift exceeds many times the experimental step size, the corresponding reference is to be discarded from the fit.

Results and Discussion

XAFS Spectra of Particulate Samples: Average Mn Valence. The normalized XANES spectra of the 12 particulated samples listed in Table 1 are shown in Figure 1. Visual examination reveals two distinct XANES patterns emerging from these exhaust particulates: group I with a single, strong absorption maximum just about the edge and group II with a doublet absorption feature at lower intensity. Samples 7−9 and 12 exhibit a group II pattern. The difference in the Fourier transforms of the extracted EXAFS signals will be shown later to correlate with the low and high Mn_3O_4 content in the groups I and II materials, respectively.

In Figure 2, the normalized XANES spectra of groups I and II particulates, typified respectively by samples 4 and 12, are plotted to show in more detail the high resolution near-edge features for comparison. The insets are the corresponding k^3-weighted Fourier transforms, which for the group I samples exhibit predominantly a nearest neighbor peak at ∼1.7 Å (phase uncorrected) and for group II samples a split nearest-neighbor peak and a strong second nearest-neighbor peak at ∼3 Å.

Figure 3 shows a linear relationship on Mn valence vs K-edge position in the selected series of manganese oxide model compounds. The edge positions with respect to the manganese metal K-edge at 6.539 keV (*20*) were obtained from position of the corresponding (fitted) arctangent step functions. The experimental edge shifts for all particulate samples listed in Table 1 fell in the range of ∼8 eV, indicating an overall average Mn valence of ∼2.2 in the exhaust materials.

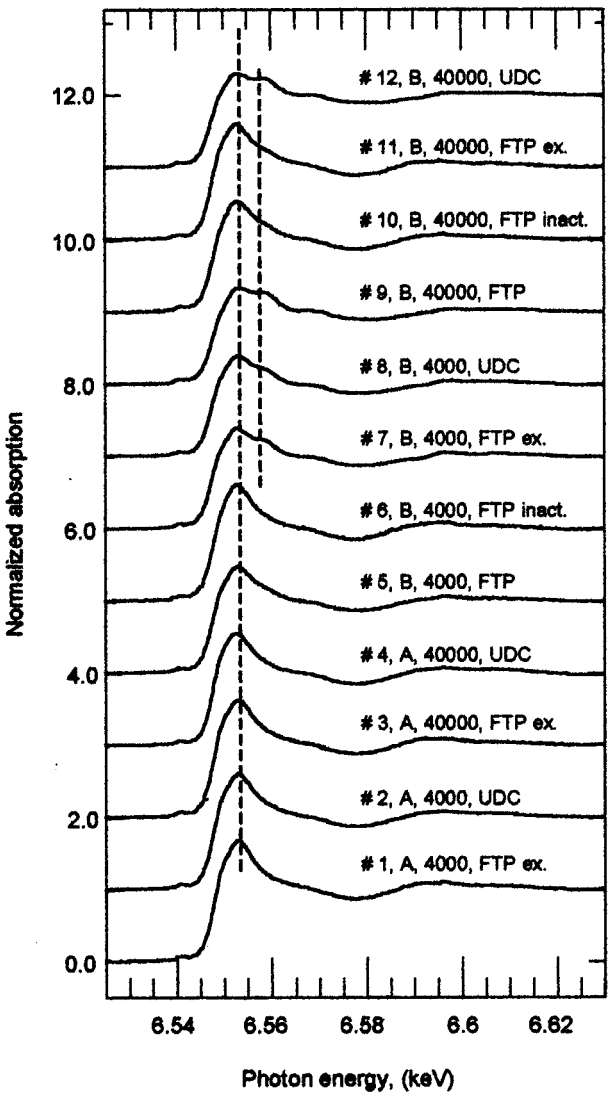

FIGURE 1. Experimental Mn K-edge XANES spectra of the 12 exhaust particulate samples. Indicated are sample no., vehicle, mileage, and test cycle (see also Table 1).

The experimental edge jumps for the particulate samples are also given in Table 1. The jump is a direct measure of the total Mn content in the sample. Some apparent trends exist. Mn content is greater for (i) UDC cycle than FTP extended as exemplified by sample 2 vs sample 1, sample 4 vs sample 3, sample 8 vs sample 7, and sample 12 vs sample 11; (ii) 40000-mi UDC than 4000-mi UDC by a factor of ∼2, as exemplified by sample 4 vs sample 2 and sample 12 vs sample 8; and (iii) FTP than FTP(inactive catalyst) by a factor of ∼3 as exemplified by sample 5 vs sample 6 and sample 9 vs sample 10. (i) and (ii) are to be expected since both more severe driving cycles, with lower fuel economy, longer accumulation mileage cycles, and more absolute fuel consumption, are expected to result in greater total exhaust particulates. The effect of inactive catalysts on lowering the Mn content in the exhaust particulates is not clear at the moment. Finally, the height of the first absorption maximum in the normalized XANES for the particulates is also listed in the Table 1. As is shown later, the intensity of this dominant XANES feature may be correlated to the concentration of Mn_3O_4 in the sample.

Mn Components Speciation: PCA Results. In this work PCA is used to determine the number and type of principal components (model compounds) that additively give rise to the set of 12 XANES spectra obtained from exhaust particu-

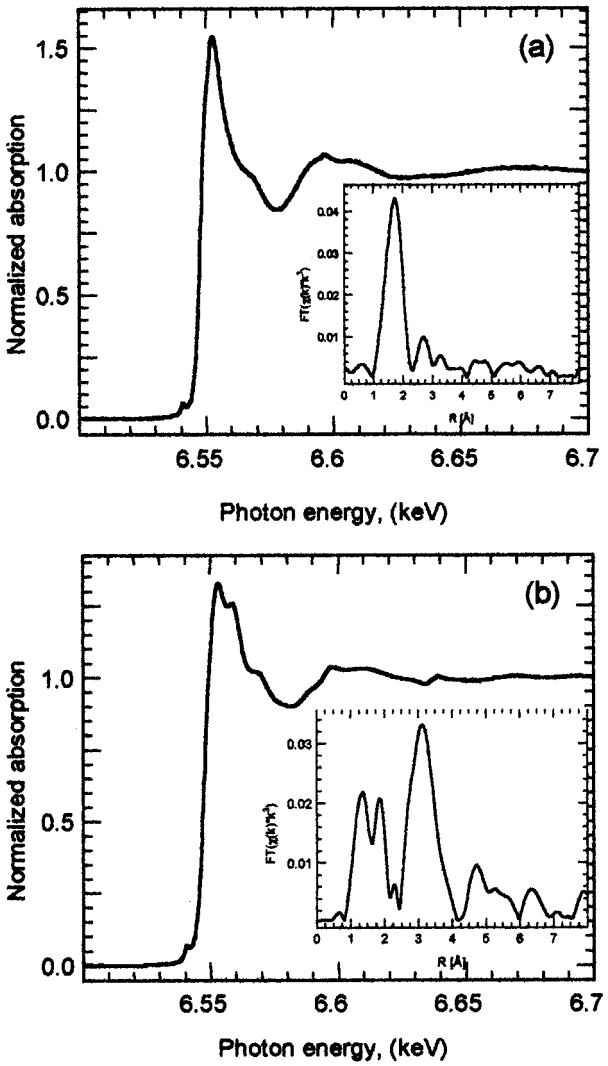

FIGURE 2. Normalized Mn K-edge XANES spectra for (a) group I and (b) group II type particulates showing a distinct doublet in the first absorption maximum feature of the latter. Insets are Fourier transforms of the corresponding EXAFS signals, which also exhibit a prominent radial structure peak at ~3 Å in the group II materials but not in the group I particulates.

lates generated under different conditions. A column matrix **A** is constructed from the 12 XANES spectra interpolated onto the same energy grid. From the eigenvalues in the SVD output matrix **V**, it is found that the first three eigenvectors of the **E** matrix are sufficient to reproduce the experimental XANES spectra with a residual of less than 1%. Hence, three principal components (i.e., manganese species) appear to be present in the exhaust particulates. In a plot of eigenvalue times weight for the first principal component versus eigenvalue times weight of the second principal component (Figure 4a), it is noted that the 12 experimental spectra are divided into two groups. These two groups are identical to the two groups described above based on the observation of whether one or two peaks in the first absorption maximum near the Mn K-edge shown in Figure 2 and shown more clearly in Figure 4b.

Target transformation was then employed to identify the probable manganese species in the exhaust particulates from the set of 10 reference compounds. These reference compounds include MnO, Mn_3O_4, Mn_2O_3, β-MnO_2, α-MnO(OH), MnS, $MnSO_4 \cdot H_2O$, $MnPO_4$, MnP_2O_7, and MnPhos. Three model compounds are found to yield a sufficient match upon

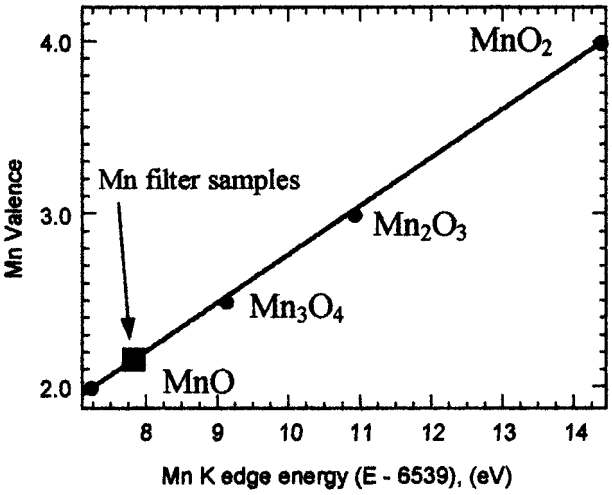

FIGURE 3. Mn valence vs experimental Mn K-edge position for model manganese oxide compounds. The solid square marks the edge positions of all 12 particulate samples.

transformation, namely, Mn_3O_4, $MnSO_4$, and MnPhos. The corresponding XANES spectra together with their transformed spectra are displayed in Figure 5a–c. On the other hand, Figure 6a,b shows the transformation results for MnO and α-MnO(OH), respectively, indicating that these two manganese species are likely not present in the analyzed exhaust particulates.

Furthermore, the singlet and doublet absorption maximum feature above the Mn K-edge of groups I and II materials may be graphically realized in a composite plot with those of the identified principal components: Mn_3O_4, $MnSO_4 \cdot H_2O$, and MnPhos. It can be seen in Figure 4b that the higher energy feature of the doublet must arise from a substantial contribution of the Mn_3O_4 component as can be shown quantitatively in the next section.

Quantification of Mn Components: Least-Squares XANES Fits. Having determined the number and type of Mn-bearing components in the 12 exhaust particulates with the PCA procedure, a nonlinear LSF procedure was then applied to quantify these components in the unknown particulate samples from their normalized experimental XANES spectra. In Figure 7, the fitted spectra (dotted lines) of a group I particulate typified by sample 1 (Table 1) and a group II particulate typified by sample 9 are superimposed with the corresponding experimental spectra (solid lines) together with the least-squares fractions of the pure model compounds making up the fitted curve. Graphically, it is obvious that the intensity of the single absorption maximum in the group I spectra is primarily a combined contribution from those of the $MnSO_4 \cdot H_2O$ and MnPhos components, whereas in the group II spectra additional contribution from the Mn_3O_4 first absorption maximum becomes significant and gives rise to a resolvable peak at higher energy—hence the doublet feature. Results of the least-squares fittings of the XANES data for the 12 particulate samples using linear combinations of the three major components Mn_3O_4, $MnSO_4 \cdot H_2O$, and MnPhos are listed in Table 2.

The XANES fit percentages given in Table 2 correspond to the amount of the respective normalized reference spectra required to yield a good match between simulated and experimental XANES spectra. Uncertainties in the fit results were estimated from a variation plot of two partial concentrations shown in Figure 8a. On the average, an uncertainty limit of 5% corresponds to an error of ca. 2.0% in the fit results.

To convert XANES fit percentages into the more commonly used weight percentages, a series of synthetic binary mixtures

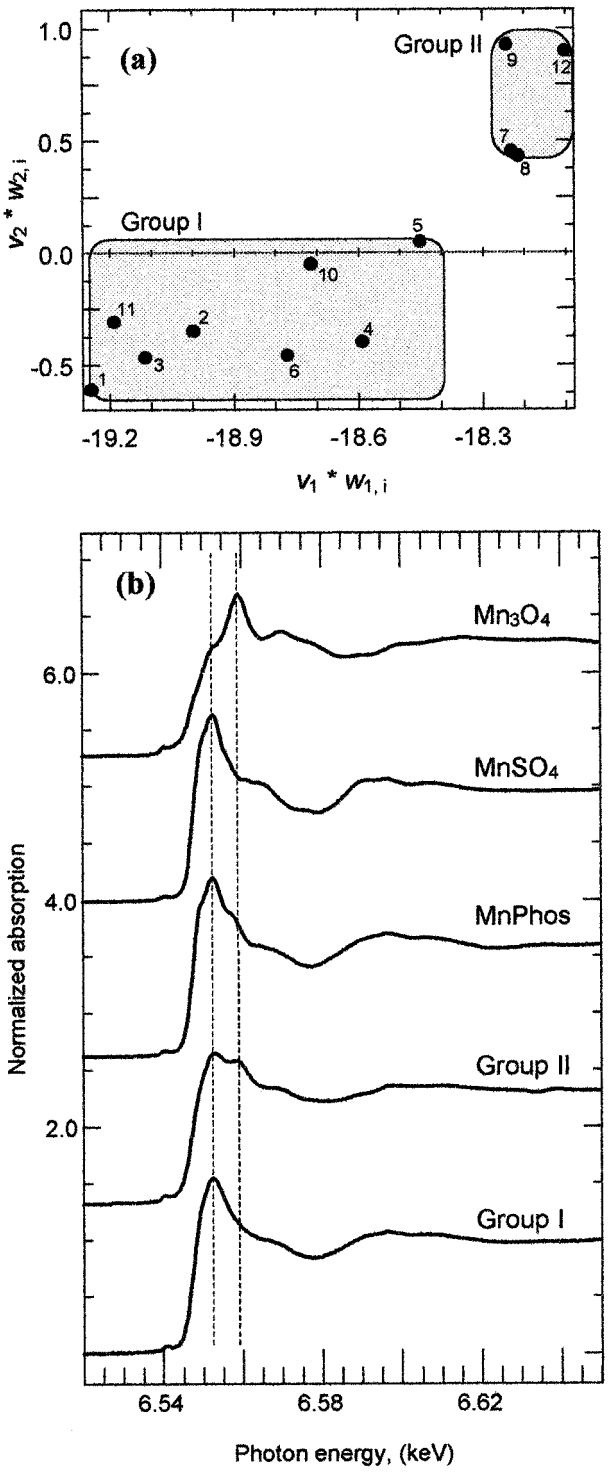

FIGURE 4. (a) Plot of PCA eigenvalues v_j times weights $w_{j,i}$ of the two most important eigenvectors obtained for the 12 exhaust particulate samples. Sample numbers are those given in Table 1. Two groups can clearly be distinguished. (b) Normalized Mn K-edge XANES spectra of the three identified Mn-bearing principal components in the auto exhaust particulates and those of the groups I and II materials, indicating origin of the high energy feature of the first absorption maximum doublet in the latter group.

of Mn_3O_4 and MnPhos was measured to generate a plot of (known) weight percent of Mn_3O_4 versus the obtained XANES fit percentage (Figure 8b). Subsequently, eq 5 was fitted to the data points and used to convert experimental XANES fit percent into weight percent of Mn_3O_4. The formalism given in eq 5 is widely used in the quantitative phase analysis of

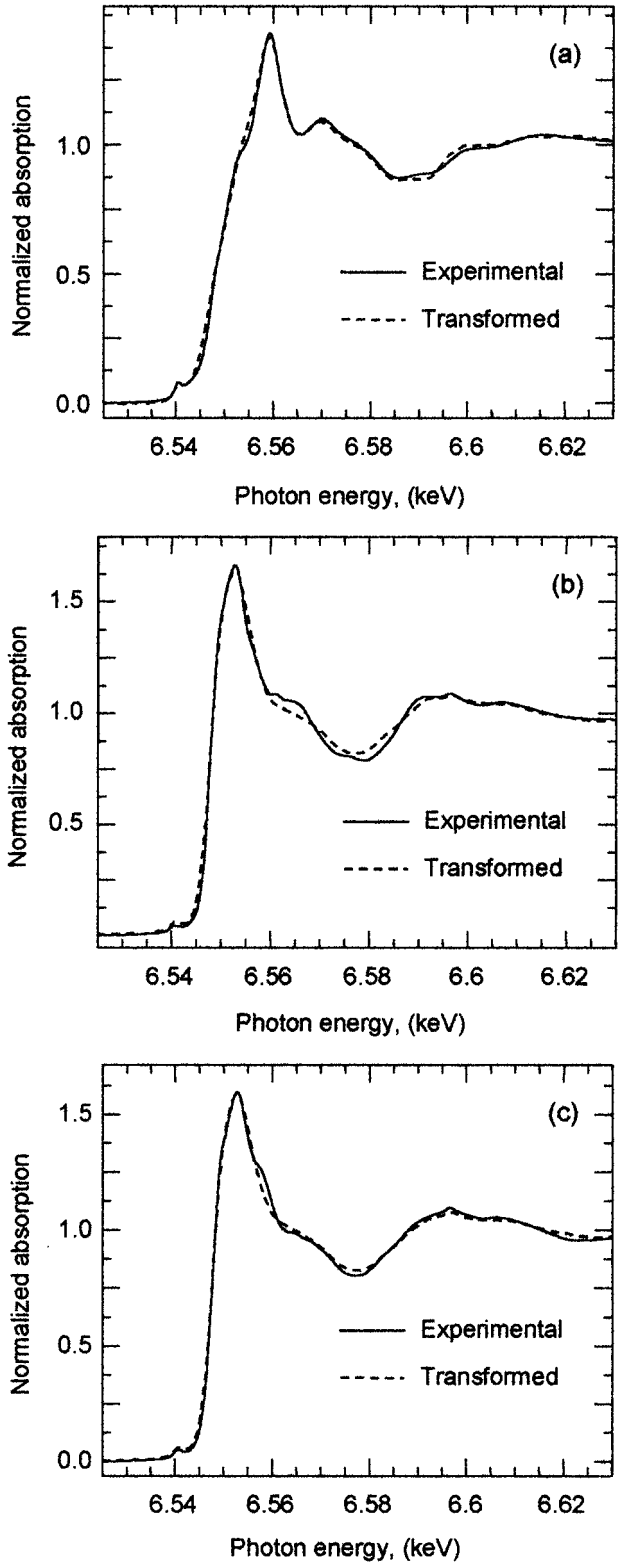

FIGURE 5. Target transformation results (dashed lines) for (a) Mn_3O_4, (b) $MnSO_4 \cdot H_2O$, and (c) MnPhos. Solid curves are the corresponding experimental XANES spectra.

X-ray diffraction data and has been described in detail in the literature (*30*):

$$\mu_{i,\mathrm{Fit}} = \frac{x_i \mu_i^*}{x_i(\mu_i^* - \mu_\mathrm{M}^*) + \mu_\mathrm{M}^*} \qquad (5)$$

where $\mu_{i,\mathrm{Fit}}$ is the Mn_3O_4 concentration determined from the

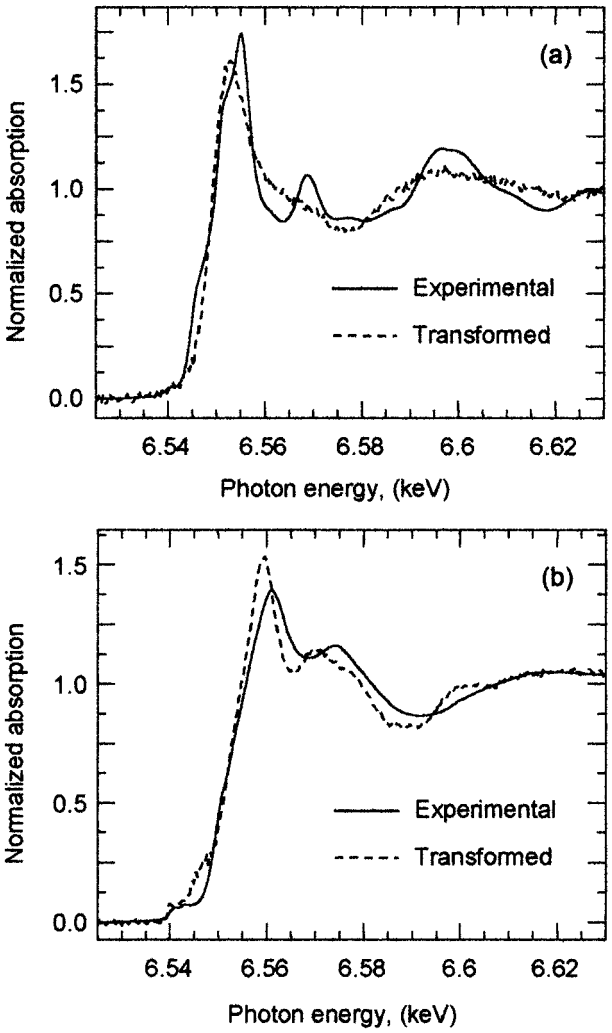

FIGURE 6. Target transformation results (dashed lines) for (a) MnO and (b) α-MnOOH, indicating that neither of these components is present in any of the 12 exhaust particulates. Solid lines are the corresponding experimental XANES spectra.

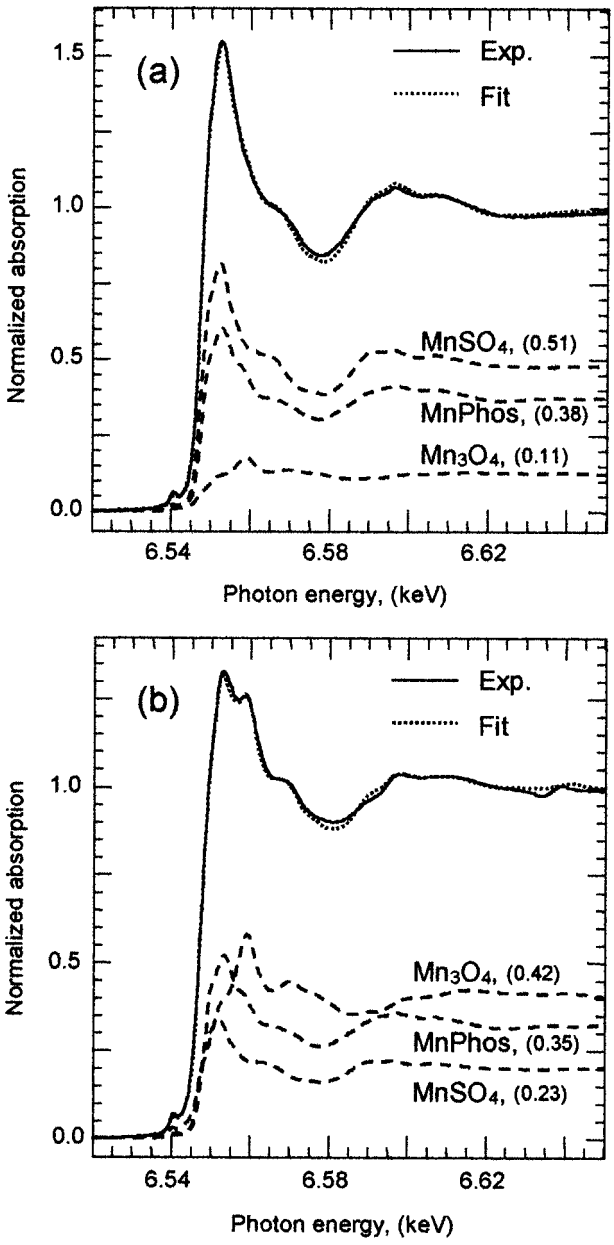

FIGURE 7. Experimental (—) and least-squares fits (···) for the Mn K-edge XANES spectra of groups (a) I and (b) II particulates. Dashed lines denote fractional contributions of the three principal components making up the fitted spectra.

least-squares fitting, x_i, the wt % μ_i* and μ_M* are the mass absorption coefficients of Mn in Mn_3O_4 and in the matrix, respectively. For Mn_3O_4, a mass absorption coefficient of 344.0 cm^2/g and for the matrix (MnPhos in the case of the mechanical mixtures), a value of 132.0 cm^2/g was obtained (*31*).

Since a simple calibration curve such as that given in Figure 8b can only be constructed for two reference substances using eq 15, the exhaust particulate samples may be treated as pseudo-binary systems consisting of $MnSO_4$ in a homogeneous matrix of $MnSO_4$/MnPhos. Hence, only weight percent of Mn_3O_4 can be obtained together with the combined weight percent of $MnSO_4$ and MnPhos. Moreover, from consideration of stoichimetry and formula weights, in synthetic binary mixtures of $MnSO_4$ and MnPhos, it was indeed found that the XANES fitting percentages almost directly correspond to weight percentages. Thus, we conclude that the weight percent ratio of $MnSO_4$ and MnPhos can be approximated by the XANES fit percent ratio of the two compounds.

Fourier transforms of the measured EXAFS signals (shown in Figure 3) are also revealing. In Figure 9, the k^3-weighted Fourier transforms of the three principal components and those of groups I and II particulates are given. Fourier transforms of group II particulates exhibit a strong peak in the 3.0-Å region, which is also prominent in that for Mn_3O_4, but not in those of the group I particulate materials. This corroborates well with the XANES simulation results summarized in Table 2.

Thus, we succeeded in speciating qualitatively and quantitatively Mn-bearing particulates emitted from automobile engines burning MMT-added gasoline using XAFS spectroscopy. The average Mn valence in the particulates is found to be ~2.2. Three principal Mn-bearing components are found to present in the particulates: Mn_3O_4, $MnSO_4 \cdot H_2O$, and MnPhos, the concentrations of which vary depending on vehicle, driving test cycles, and mileage accumulation. The sources of S and P in the exhaust particulates are known to arise from ZDDP (zinc dialkyl dithiophosphate) additives in lubriant oil used to generate antiwear films on steel surfaces in the cylinders (*32*, *33*). Group I particulates are high in $MnSO_4 \cdot H_2O$ and MnPhos and low in Mn_3O_4 content (4−9 wt %), and group II particulates are high in Mn_3O_4 (15−22 wt %).

TABLE 2. Type and Amount of Mn-Bearing Species in Exhaust Particulates Derived from a Combination of PCA and Least-Squares Fitting of XANES Spectra

no.	vehicle	mileage	test cycle	Mn_3O_4 (%)	$MnSO_4$ (%)	MnPhos (%)	group	Mn_3O_4 (wt %)	Σ (wt %)[a]
1	A	4 000	FTP extended	11	51	38	I	4	96
2	A	4 000	UDC	18	33	49	I	8	92
3	A	40 000	FTP extended	16	39	45	I	7	93
4	A	40 000	UDC	10	35	55	I	4	96
5	B	4 000	FTP	20	34	46	I	9	91
6	B	4 000	FTP inactive catalyst	7	48	45	I	3	97
7	B	4 000	FTP extended	32	23	45	II	15	85
8	B	4 000	UDC	30	25	45	II	14	86
9	B	40 000	FTP	42	23	35	II	21	79
10	B	40 000	FTP inactive catalyst	17	39	44	I	8	92
11	B	40 000	FTP extended	21	50	29	I	9	91
12	B	40 000	UDC	43	24	33	II	22	78

[a] Σ = $MnSO_4$ weight percent + MnPhos weight percent.

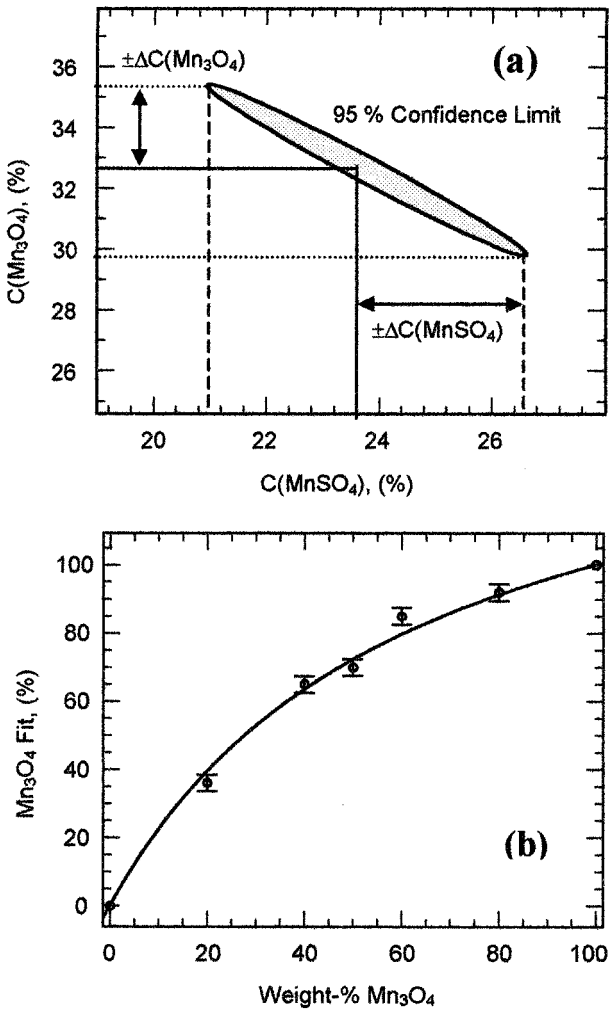

FIGURE 8. (a) Variation plot of partial concentration of Mn_3O_4 vs concentration of $MnSO_4 \cdot H_2O$ obtained for sample 4. Solid curve indicates area in parameter space that corresponds to a variation in fit residual *R* of <5%. Extension of ellipse on both axes was used to estimate the uncertainty, $\pm\Delta C$, in least-squares fit results. (b) Calibration curve obtained from fitting eq 5 to weight percent of Mn_3O_4 vs % of XANES fit for a series of binary Mn_3O_4−MnPhos synthetic mixtures.

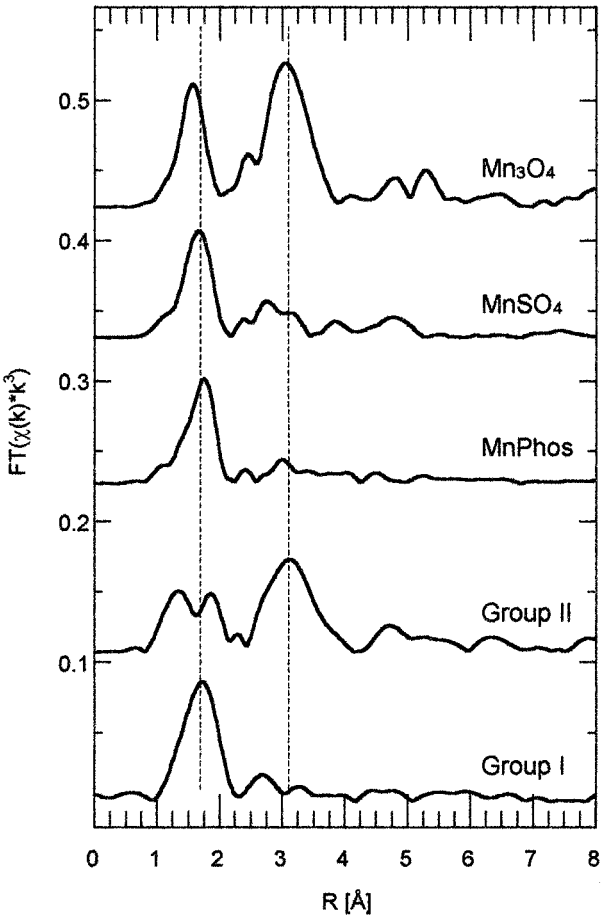

FIGURE 9. k^3-weighted Fourier transforms of the three principal components found to contain both groups I and II particulates. It is clearly seen that the 3-Å peak in the group II materials arises from a substantial contribution from Mn_3O_4 (Table 2).

The work reported herein demonstrates a powerful combination of the PCA and LSF procedure for meaningful qualitative (number and type of components) and quantitative analysis of unknown mixtures from XANES data and clearly establishes XAFS spectroscopy as a quantitative analytical tool for speciation of dilute, multicomponent systems of environmental relevance.

Acknowledgments

The XAFS measurements were carried out at Stanford Synchrotron Radiation Laboratory (SSRL), supported by the Chemical Division of the U.S. Department of Energy (DOE). We thank S. R. Wasserman for helpful discussions on the PCA algorithm and its implementation. T.R. is grateful to the

Alexander-von-Humboldt Foundation for a Feodor Lynen Research Fellowship. This publication is based on a study sponsored and founded by Ethyl Corporation, preliminary results of which have been previously submitted to the U.S. Environmental Protection Agency by Ethyl Corp.in satisfaction of registration requirements arising under Section 211(a) and (b) of the Clean Air Act and corresponding regulations of 40 CFR Section 79.50 et seq.

Literature Cited

(1) Abelson, P. H. *Science* **1998**, *281*, 1609.
(2) Mckinsey, K. *Sci. Am*. **1998**, *June*, 53.
(3) Lytle, C. M.; Smith, B. N.; McKinnon, C. Z. *Sci. Total Environ*. **1995**, *162*, 105.
(4) Pellizzari, E. D.; Clayton, C. A.; Rodes, C. E.; Mason, R. E.; Piper, L. L.; Fort, B.; Pfeifer, G.; Lynam, D. *Atmos. Environ*. **1999**, *33*, 721.
(5) EPA. *Comments on the use of MMT in Unleaded Gasoline*; Office of Research and Development: Washington, DC, 1990.
(6) EPA. *Reevaluation of Inhalation Health Risks Associated with MMT in Gasoline*; Office of Research and Development: Washington, DC, July 1, 1994.
(7) Preuss, P. W. *EPA Air Dockets A-93-26, II-A-16 and A-93-26, II-A-18*; Office of Research and Development: Washington, DC, December 16, 1991, and July 13, 1994.
(8) Colmenares, C.; Deutsch, S.; Evans, C.; Nelson, A. J.; Terminello, L. J.; Reynolds, J. G.; Roos, J. W.; Smith, I. L. *Appl. Surf. Sci*. **1999**, *151*, 189−202.
(9) Koningsberger, D. C., Prins, R., Eds. *X-ray Absorption: Principles, Applications, Techniques of EXAFS, SEXAFS and XANES*; Wiley-Interscience: New York, 1988.
(10) Rehr, J. J.; Albers, R. C.; Zabinsky, S. I. *Phys. Rev. Lett*. **1992**, *69*, 3397.
(11) Rehr, J. J.; Booth, C. H.; Bridges, F.; Zabinsky, S. I. *Phys. Rev*. **1994**, *B49*, 12347.
(12) Pickering, I. F.; Brown, G. E., Jr. *Environ. Sci. Technol*. **1995**, *29*, 2456.
(13) Foster, A. L.; Brown, G. E.; Tingle, T. N.; Parks, G. A. *Am. Mineral*. **1998**, *8*, 553.
(14) O'Day, P. A.; Carroll, S. A.; Waychunas. G. A. *Environ. Sci. Technol*. **1998**, *32*, 943.
(15) Ostergren, J. D.; Brown, G. E., Jr.; Parks, G. A.; Tingle, T. N. *Environ. Sci. Technol*. **1999**, *33*, 6627.
(16) Morin, G.; Juillot, F.; Ostergren, J. D.; Ildefonse, P.; Calas, G.; Brown, G. E., Jr. *Am. Mineral*. **1999**, *84*, 420.
(17) Roos, J. W. Personal communication.
(18) Karpenko, V.; Kinney, J. H.; Kulkarni, S.; Neufeld, K.; Poppe, C.; Tirsell, K. G.; Wong, J.; Cerino, J.; Troxel, T.; Yang, J. *Rev. Sci. Instrum*. **1989**, *60*, 1451.
(19) Lytle, F. W.; Greegor, R.; Sandstrom, D. R.; Marques, E. G.; Wong, J.; Spiro, C. L.; Huffman, G. P.; Guggin F. E. *Nucl. Instrum. Methods* **1984**, *229B*, 5870.
(20) Frahm, R. *Nucl. Instrum. Methods* **1988**, *A270*, 578.
(21) Ressler, T. *J. Synchrotron Radiat*. **1998**, *5*, 118.
(22) Wong, J.; Lytle, F. W.; Messmer, R.; Maylotte, D. H. *Phys. Rev. B* **1984**, *30*, 5596.
(23) Bearden, J. A.; Burr, A. F. *Rev. Mod. Phys*. **1967**, *39*, 135.
(24) Fay, M. J.; Proctor, A.; Hoffmann, D. P.; Houalla, M.; Hercules, D. M. *Mikrochim. Acta* **1992**, *109*, 281−293.
(25) Wasserman, S. R. *J. Phys. IV* **1977**, *C2*−203.
(26) Press: W. H.; Flannery, B. P.; Teukolsky, S. A.; Vetterling, W. T. *Numerical Recipes in C*; Cambridge University Press: Cambridge, 1989.
(27) Malinowski, E. R. *Factor Analysis in Chemistry*, 2nd ed.; John Wiley: New York, 1991.
(28) Forsythe, G. E.; Malcolm, M. A.; Moler, C. B. *Computer Methods for Mathematical Computations*; Prentice Hall: Englewood Cliffs, NJ, 1977.
(29) Stoer, J.; Bulirsch, R. *Introduction to Numerical Analysis*; Springer-Verlag: New York, 1980.
(30) Klug, H. P.; Alexander, L. E. *X-ray Diffraction Procedure for Polycrystalline and Amorphous Materials*, 2nd ed.; Wiley: New York, 1974.
(31) McMaster, W. H.; Kerr Del Grande, N.; Mallet, J. H.; Hubbell, J. H. Lawrence Radiation Laboratory Report UCRL-50174, Sec. 2 Rev., 1974.
(32) Yin, Z.; Kasrai, M.; Fuller, M.; Bancroft, G. M.; Fyfe, K.; Tan, K. H. *Wear* **1997**, *202*, 172 and 192.
(33) Kasrai, M.; Culter, J. N.; Gore, K.; Canning G.; Bancroft G. M. *Tribol. Trans*. **1998**, *41*, 69−77.

Received for review July 14, 1999. Revised manuscript received December 6, 1999. Accepted December 23, 1999.

ES990787X